Geophys. J. Int. (2005) **163,** 79–89 doi: 10.1111/j.1365-246X.2005.02724.x

Retracking ERS-1 altimeter waveforms for optimal gravity field recovery

David T. Sandwell[1] and Walter H. F. Smith[2]

[1] *Scripps Institution of Oceanography, La Jolla, CA* 92093-0225*, USA*
[2] *National Oceanic and Atmospheric Administration, Silver Spring, MD* 20910*, USA*

Accepted 2005 July 27. Received 2005 June 6; in original form 2004 December 8

SUMMARY

We have reprocessed ERS-1 radar altimeter waveforms using an algorithm designed to minimize sea surface slope error and decouple it from significant wave height (SWH) error. Standard waveform retracking estimates three parameters—arrival time, SWH and amplitude. We show that errors in retracked estimates of arrival time and SWH are inherently correlated because of the noise characteristics of the returned waveform. This suggests that some of what is called 'sea state bias' in the literature may be caused by correlated errors rather than true electromagnetic or skewness bias. We have developed a retracking algorithm that reduces this error correlation and makes the resolution of sea surface slope signals independent of sea state. The main assumption is that the SWH varies smoothly along the satellite track over wavelengths of 90 km. This approach reduces the rms error in sea surface slope to only 62 per cent of that of standard retracking methods. While our method is optimized for gravity field recovery, it may also improve the resolution of sea surface height signals of interest to physical oceanographers.

Key words: gravity anomaly, radar altimetry.

INTRODUCTION

Satellite radar altimetry has become an important tool for investigating the tectonics of the ocean basins, especially in areas of sparse ship coverage. The ocean surface is nearly an equipotential surface of gravity, so high spatial resolution maps of ocean surface topography can be converted to gravity anomalies and even used to predict regional variations in seafloor depth (Smith & Sandwell 1997). Further improvement in the accuracy and resolution of the marine gravity field will require more precise altimeter measurements and/or a longer duration mission to minimize the various noise sources. For recovery of the static marine gravity field, the critical measurement is the slope of the ocean surface. Laplace's equation combined with Bruns' formula shows that one microradian (μrad) of ocean surface slope roughly corresponds to 1 milligal (mGal) of gravity anomaly. Ocean surface slope can be estimated by differencing height measurements along satellite altimeter profiles, so absolute range accuracy is largely irrelevant. Indeed the usual corrections and ancillary data that are needed to recover the temporal variations in ocean surface height associated with currents and eddies are largely unimportant for the recovery of the gravity field because the slope of these corrections is far less than the slope error in the radar altitude measurement.

Consider the recovery of a 1 mGal accuracy gravity anomaly having a wavelength of 28 km. This requires a sea surface slope accuracy of 1 μrad over a 7-km-length scale (1 s of flight along the satellite track), necessitating a height precision of 7 mm in one-per-second measurements of sea surface height. Current satellite altimeters such as Geosat, ERS-1/2 and Topex have typical 1-s averaged range precision of 30–40 mm resulting in gravity field accuracies of 4–6 mGal. There are three ways to improve the gravity field accuracy. First, one could design and fly a new radar altimeter with inherently better range precision than the current generation of altimeters (Raney *et al.* 2004). Second, one could make multiple measurements of ocean surface slope. The currently available non-repeat ocean altimeter measurements come from 1.5 yr of Geosat during its Geodetic Mission and 1 year of ERS-1 during its geodetic phase. Third, one could improve the range precision of the existing measurements.

Maus *et al.* (1998) took the third approach, developing and implementing a new waveform retracking algorithm that significantly improves the precision and along-track resolution of the ERS-1 altimeter data. Their algorithm operates on multiple waveforms and imposes a smoothness criterion for the multiple arrival times within the group. More important, they use a single rise-time parameter for the group to stabilize the recovery of the arrival times. While their paper provides a recipe for improving range precision with respect to standard retracking methods, they do not fully discuss the assumptions of their method and the physical meaning of constrained parameters in their approach.

In this paper we develop our own retracking approach. Our results confirm the analysis and recommendations of Maus *et al.* (1998), and clarify why that approach works well. However, our approach does not require simultaneous inversion of multiple waveforms, and

we also do not require a smoothness constraint on arrival times; our only constraint is that the rise-time parameter must vary smoothly along the satellite's ground track. Physically this corresponds to the assumption that the sea surface roughness, due to ocean waves and swell, varies smoothly in space. Our approach is easier to implement on a small computer, as the non-linear least-squares inversion operations are done only one waveform at a time. Further, the correlation length scales in the rise-time and amplitude parameters are explicitly adjustable in our technique, giving physical insight and meaning to the tuned parameters.

Here we investigate the general problem of correlated errors and sea state bias, to show the motivation for our retracking scheme. Our strategy for reducing those errors obtains a significantly reduced error variance, but more importantly, the spatial resolution of data processed by our method is independent of sea state. These results may be applied to ocean data from any satellite radar altimeter and should have wide application. Using our method, we have retracked the ERS-1 altimeter waveform data for all of the geodetic phase and part of the 35-day-repeat phase, and we will make these retracked data available to the scientific community. This paper, therefore, also contains an investigation of the expected error distribution in ERS-1 waveforms caused by a unique feature of the ERS-1 hardware. We are also experimenting with retracking all of the Geosat altimeter data using similar methods. Geosat has its own unique peculiarities, which will be the subject of another paper.

A MODEL FOR THE RETURNED OCEAN WAVEFORM AND ITS EXPECTED NOISE

To understand the assumptions and technique for improving the range precision, we start with a simplified discussion of how a radar pulse interacts with the ocean surface. For a more complete treatment of the engineering aspects of radar design and ocean reflection characteristics see the primary references (Brown 1977; Hayne 1980; MacArthur *et al.* 1987; Hayne *et al.* 1994; Rodriguez & Martin 1994; Chelton *et al.* 2001; Amarouche *et al.* 2004). The radar altimeter emits a short pulse, or more precisely, a frequency-modulated chirp that reflects from the ocean surface and returns to the antenna. The recorded power is the double convolution of the system point target response with the ocean surface height distribution and the two-way antenna pattern. The height distribution of ocean waves is well approximated by a Gaussian function (Stewart 1985); if the point target response is also approximated with a Gaussian form then the form of the return power is well approximated by an error function with a slow decay of the trailing edge due to the finite antenna beam width. A model for the expected power versus time is (Brown 1977; Amarouche *et al.* 2004).

$$M(t, t_o, \sigma, A) = \frac{A}{2}[1 + \mathrm{erf}(\eta)] \begin{cases} 1, & t < t_o \\ \exp[-(t - t_o)/\alpha], & t \geq t_o \end{cases}, \quad (1)$$

where

$$\eta = \frac{(t - t_o)}{\sqrt{2}\sigma}, \quad (2)$$

and where t is the time since the pulse was transmitted, t_o is the arrival time of the half power point of the returned energy, σ is the arrival rise-time parameter, A is the amplitude of the returned waveform, and α is an exponential decay in the trailing edge due to the finite beam width of the antenna. In addition to these four parameters, waveforms from some altimeters also show a background noise level.

The pointing accuracy of the ERS spacecraft was generally very good and the antenna mispointing was much less than the antenna beam width, so we set this decay parameter α to a constant (137 nsec). The ERS-1 altimeter hardware truncated small power levels to zero (discussed below), and so we do not need a background noise level parameter. Therefore our retracking model for ERS-1 has only three free parameters, A, t_o and σ. The automatic gain control loop in hardware maintained A at a relatively constant level, and the significantly variable parameters of chief concern in this paper are t_o and σ. In our model fitting, these are treated as non-dimensional parameters in dimensionless units of waveform sample gate widths; the physical time sampled by an ERS-1 waveform gate sample is 3.03 ns of two-way travel time, corresponding to 0.4545 m of range to the sea surface. The rise width of the waveform, σ, is a convolution of the effective width of the point target response and the vertical distribution of ocean surface waves, usually parameterized in terms of a Gaussian standard deviation equal to one-fourth of the significant wave height, SWH. An example model waveform for $\sigma = 6.67$ ns (significant wave height of 3.6 m) is shown in Fig. 1 (upper).

The objective of our analysis is to reduce the error in the estimated arrival time of the pulse, t_0. However, before considering this problem one must understand the signal and noise characteristics of the return waveform. The ERS radar altimeter emits 1020 pulses per second and the returned power P_i is recorded in 64 gates spaced at 3.03 ns. An onboard tracker is used to keep the pulse approximately centred in the traveltime window (gate 32) while 50 returned pulses are averaged. The averaged returned waveforms are available from the European Space Agency in the 'WAP' data product, which also contains the onboard tracker's estimate of the expected range to the ocean surface used to align the waveforms.

An individual radar pulse reflects from numerous random scatterers on the ocean surface so the return power versus time will be noisy—essentially following a Rayleigh scattering distribution. This high noise level is reduced in the 50 waveform average. Assuming the speckle is incoherent from pulse to pulse, this incoherent average will reduce the speckle noise by a factor of $\sqrt{50}$. Ideally, in averaging 50 values one first sums the individual contributions and then divides the sum by 50. However, to avoid overflow in the ERS-1 hardware, each waveform gate sample was first divided by 50, the result truncated downward to an integer, and then the truncated value added to the accumulating sum. Since each waveform contains random fluctuations the effect of this hardware truncation can only be investigated with a Monte Carlo simulation (Appendix A). We have found that expected mean power levels below about 23 will be truncated to zero, so the emergent leading edge of the pulse is lost. The averaging of 50 pulses combined with the truncation issue leads to the following functional form for the uncertainty in the power W_i as a function of the recorded power P_i

$$W_i = \frac{(P_i + P_o)}{\sqrt{K}}, \quad (3)$$

where K is the number of statistically independent waveforms used in the average and P_o is the offset due to the truncation. Our Monte Carlo simulation of the truncation process and our experiments in optimizing the retracking of real ERS waveforms led us to use $K = 44$ and $P_o = 50$, which is essentially the same weighting used by Maus *et al.* (1998). While the results are largely insensitive to the exact numerical values for K and P_o, the functional form of this uncertainty leads to a high correlation between the arrival time

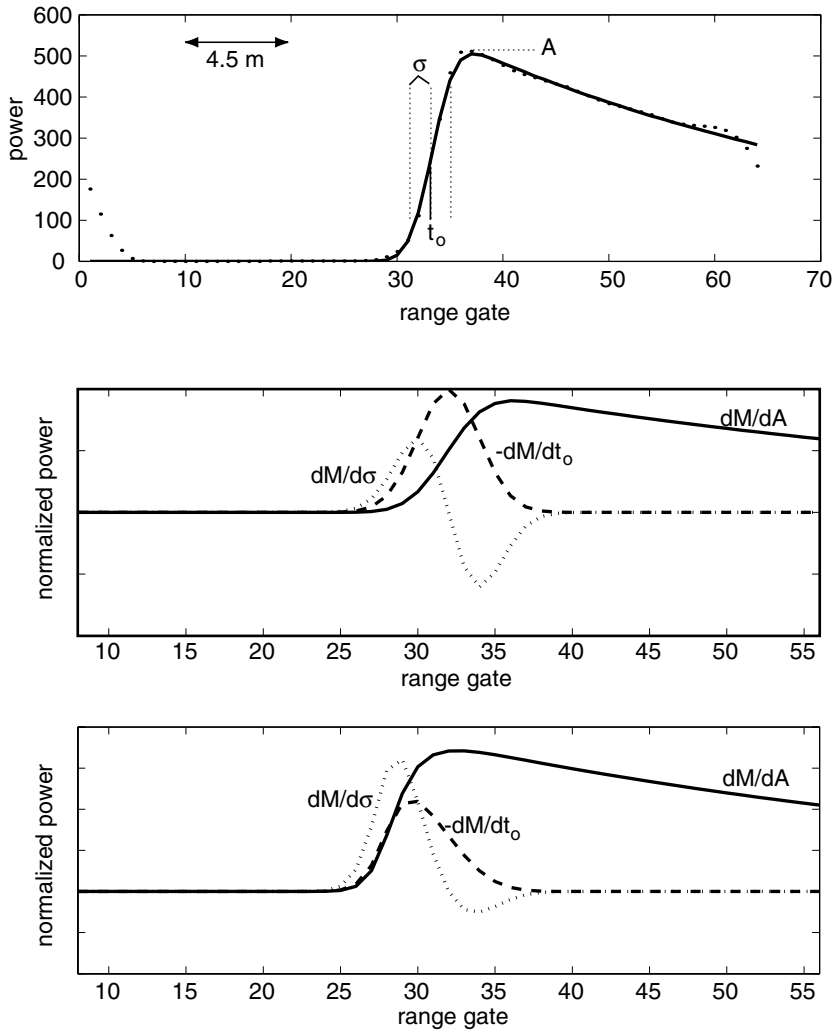

Figure 1. Upper—average of 10 000 ERS-1 radar waveforms (dotted) and a simplified model (solid, equation 1) with three adjustable parameters: A—amplitude, t_o—arrival time, and σ—rise time. Time parameters are measured in dimensionless waveform gate widths equal to 3.03 ns of two-way travel time or 454 mm of range to the sea surface. middle—partial derivatives of model (eq. 1) with respect to A (solid), t_o (dashed) and σ (dotted) versus gate number. Note the functions dM/dt_0 and $dM/d\sigma$ are orthogonal. Lower—partial derivatives of the model waveform weighted by the expected uncertainty in the power (eq. 3). Note the functions dM/dt_0 and $dM/d\sigma$ appear similar. This leads to a high correlation between arrival time and rise time during the least-squares estimation.

and the rise time when they are estimated using a weighted least-squares approach. Overcoming this correlation is the essence of our study.

LEAST-SQUARES MODEL FITTING: CORRELATED MODEL ERRORS

A standard least-squares approach is used to estimate the three parameters (t_o, σ and A). Because the problem is non-linear in arrival time and SWH, we use an iterative gradient method. The chi-squared measure of misfit is

$$\chi^2 = \sum_{i-1}^{N} \left[\frac{P_i - M_i(t_o, \sigma, A)}{W_i} \right]^2, \tag{4}$$

where N is the number of gates used for the fit and M_i is the model evaluated at the time of the ith gate. One starts the iteration by subtracting a starting model based on parameters t_o^o, σ^o and A^o. The updated model parameters t_o^1, σ^1 and A^1 are found by solving the following linear system of equations

$$\begin{bmatrix} P_1' \\ P_2' \\ \vdots \\ \vdots \\ P_N' \end{bmatrix} = \begin{bmatrix} \frac{\partial M_1}{\partial t_o} & \frac{\partial M_1}{\partial \sigma} & \frac{\partial M_1}{\partial A} \\ \vdots & \vdots & \vdots \\ \vdots & \vdots & \vdots \\ \frac{\partial M_N}{\partial t_o} & \frac{\partial M_N}{\partial \sigma} & \frac{\partial M_N}{\partial A} \end{bmatrix} \begin{bmatrix} t_o^1 - t_o^o \\ \sigma^1 - \sigma^o \\ \vdots \\ A^1 - A^o \end{bmatrix}, \tag{5}$$

where P_i' is the waveform power minus the model from the previous iteration. The derivatives of the model with respect to the parameters are

$$\frac{\partial M}{\partial t_o} = \frac{-A}{\sigma\sqrt{2\pi}} e^{-\eta^2}, \tag{6}$$

$$\frac{\partial M}{\partial \sigma} = \frac{-A}{\sigma\sqrt{\pi}} \eta e^{-\eta^2},$$

$$\frac{\partial M}{\partial A} = \frac{M}{A}.$$

We have not included the complications of the exponential decay in the partial derivatives of eq. (1) because this effect is largely removed with the starting model, and because residual misfits in the plateau of the waveform are chiefly random and do not significantly drive the fit of the three important parameters. These partial derivatives are shown in Fig. 1 for the case of an unweighted and weighted least-squares adjustment. A standard Newton iteration algorithm is used to determine the three model parameters (t_o, σ, A) that minimize the rms misfit.

An interesting feature of this least-squares problem is an inherent correlation between errors in estimated arrival time and errors in estimated rise time. We explore this with Monte Carlo experiments simulating model fitting to noisy data. In an experiment we generate 2000 realizations of noisy waveforms, each waveform having the

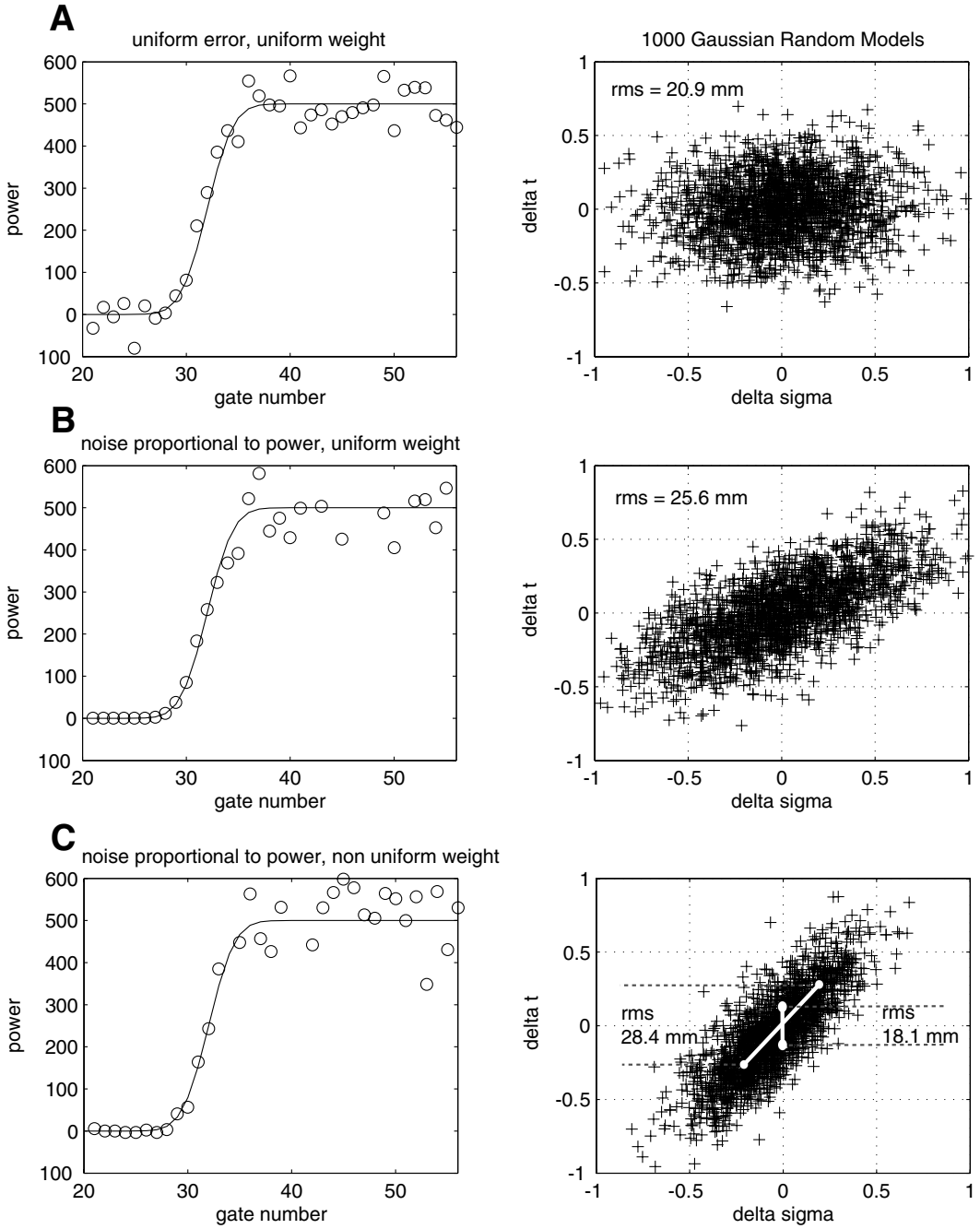

Figure 2. Simulations of least-squares parameter estimation. For each case (A, B, C) 2000 random models were constructed by adding noise to the exact model waveform (solid curve left plots) and a non-linear least-squares approach was used to recover the model parameters. Right plots show errors in estimation of arrival-time (delta t) and rise-time (delta sigma) parameters. Case A with uniform noise and uniform weight has no correlation between arrival time and rise time (rms-arrival-time error equivalent to 20.9 mm in sea surface height). Case B with noise proportional to power and uniform weight has some correlation between arrival time and rise-time (rms-arrival-time error 25.6 mm of height equivalent). Case C with noise proportional to power and weight inversely proportional to power has high correlation between arrival time and rise time (rms-arrival-time error 28.4 mm in height). If the rise-time parameter were known the rms error in arrival time could be reduced to 18.1 mm of height, corresponding to a 36 per cent reduction in noise.

same known true parameters for arrival time, rise time and amplitude, plus an independent realization of random noise. We then do a least squares fit to each waveform, obtaining 2000 noisy estimates of each model parameter, and we examine the error distribution in these estimated parameters. The results of these experiments are shown in Fig. 2, for each of three different cases we examined: experiment 'A' employs constant waveform error and uniform least-squares weighting; experiment 'B' employs waveform error proportional to waveform power but uniform least-squares weighting; and experiment 'C' has waveform error and least-squares weight both proportional to waveform power.

First consider experiment 'A', the physically unrealistic case where the waveform noise is uniform across all gates. Noise in the waveform power introduces an error in all three estimated parameters. The simulation shows that the error in rise time and arrival-time are uncorrelated, and for this case, the rms uncertainty in the arrival-time estimate is equivalent to 20.9 mm of uncertainty in resolved sea surface height (Fig. 2a).

It is physically more realistic to consider cases in which the received waveform noise is proportional to the received power (eq. 3). In this situation we may choose to make a uniformly weighted least-squares fit, setting all W_i equal in eq. (4) (effectively an unweighted fit), or we may choose non-uniform weighting, substituting (3) in (4), (a weighted fit). Our simulations of these two cases are experiments 'B' (unweighted) and 'C' (weighted).

In the unweighted case (Fig. 2b) the simulation shows a correlation between rise time and arrival time and rms uncertainty in the arrival time has increased to 25 mm of height equivalent. More important, the two parameters are now correlated so a positive error in the estimate of rise time will produce a positive error in the estimate of arrival time. Since rise time and arrival time are related to the physical parameters of SWH and sea surface height, the inherent correlation has the same effect as the so-called sea state bias. True electromagnetic (EM) bias occurs because more energy reflects from the troughs of the waves than from the crests so arrival time increases with increasing SWH. The simulation shows the same type of behaviour. Indeed we suggest that the so-called sea state bias (different for each altimeter, Scharroo & Lillibridge 2005) consists of a true EM bias and an artificial bias that is related to the least-squares estimation approach as well the noise response characteristics of the radar instrument.

Finally we consider the case of a weighted least-squares estimate of the three waveform parameters (Fig. 2c). Maus *et al.* (1998) proposed that to obtain an improved estimate of the arrival time one should weight the least-squares adjustment where the gates with higher noise (i.e. higher power) are down weighted (eqs 3 and 4). We remark that in theory, this weighted least-squares approach should yield the maximum likelihood model parameters if there is no gate-to-gate or waveform-to-waveform correlation of the waveform errors. This weighted approach is the basis of the 'SMLE' retracker used by the European Space Agency to make the 'OPR' retracked data product. However, in this case our simulations and previous studies (Dumont 1985; Rodriguez 1988), show even a more severe correlation between rise time and arrival time having a slope of 1, which translates into a sea state bias of nearly 25 per cent. We confirmed this effect by retracking ERS-1 data using the three-parameter weighted least-squares approach and then determining the sea state bias that provides the best rms match between retracked sea surface slopes and slopes of the GFSC00 mean sea surface model (Wang 2000). The analysis of real data requires a 23 per cent SSB for best fit. Note when the sea state bias is estimated for heights rather than slopes, the best SSB is about 8 per cent. This is because the errors in the SWH primarily occur at short wavelengths which are enhanced in the slope profiles. In addition to the adverse correlation of the weighted least-squares approach, the rms error in the arrival time increases to 28.4 mm of height equivalent, which is worse than the case of uniform weight.

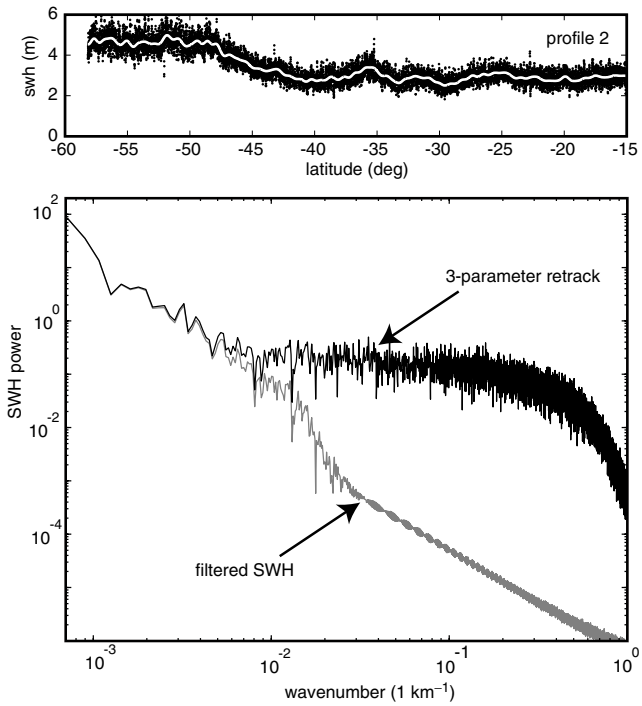

Figure 3. Upper—SWH profile across the South Pacific Ocean derived from the 3-parameter retracking algorithm. Lower—Power spectrum of SWH for six profiles shows a noise floor intersecting the SWH signal at a wavelength of about 100 km. We filter the SWH using a Gaussian filter with a 0.5 gain at 90-km wavelength (grey curves upper and lower) to provide a stable estimate of SWH for the 1-parameter retracking algorithm.

APPROACHES TO REDUCE THE SEA SURFACE HEIGHT ERROR

Assume for the moment that the true rise time and amplitude were known *a priori* so that the least-squares model fit could be performed for only one parameter, the arrival time. This case is illustrated in Fig. 2(c) where we have assigned zero error to our rise-time estimate. For this one-parameter model, the rms in the arrival time is reduced to 18.1 mm of height equivalent. This is a 30 per cent improvement over the three-parameter unweighted solution and nearly a 40 per cent improvement over the three-parameter weighted solution. Therefore if the rise time, or equivalently, the SWH was known *a priori*, then the arrival time could be measured more precisely which would lead to an improved estimate of slope and ultimately gravity anomaly.

To achieve this objective, we assume that the SWH varies smoothly along each satellite profile. There is a physical basis for making the assumption—at least in the deep ocean. Spatial variations in SWH will depend on convolution of temporal variations in wind forcing with the wave group velocity (6–12 m s^{-1}). Typically a storm takes a day or so to pass over a fixed point and during this time the surface waves will travel 500–1000 km usually outrunning the storm. Therefore, SWH should be very smooth over length scales less than

a few hundred kilometres. The assumption will break down as the waves approach depths comparable to their wavelength ~300 m, since the amplitudes will increase and the wavelength will shorten over distances related to the bathymetric gradient. Therefore, the assumption will not be as good in coastal areas. Monaldo (1988) found correlation scales of order 100 km in the SWH field.

Our overall approach for minimizing error in sea surface slope is to: (1) retrack each waveform (or several waveforms) independently using the full three-parameter model, (2) smooth the rise-time and amplitude parameters in the along-track direction with a low-pass filter and (3) retrack the data again using the smoothed rise time and amplitude as *a priori* constraints in the more precise one-parameter fit for arrival time only. The appropriate low-pass filter wavelength for the rise-time parameter was determined through a power spectral analysis of six altimeter profiles crossing the Pacific basin. An example is shown in Fig. 3 where the SWH power decreases with increasing spatial frequency until 0.01 cyc-km^{-1}. At higher wavenumbers the power is relatively flat and we interpret this as white noise caused by errors in our estimate of the rise-time parameter; to suppress this noise we have adopted a Gaussian low-pass filter with a 0.5 gain at 90 km full wavelength. In addition to smoothing the rise-time parameter prior to retracking, we also smooth the amplitude but over a shorter wavelength, using a Gaussian low-pass filter with a 0.5 gain at 14 km full wavelength. This length is slightly less than the characteristic length scale of a noise resonance in the onboard alpha/beta tracking software that adjusts the tracking parameters and gain onboard the satellite (Rodriguez & Martin 1994).

IMPROVEMENTS IN PRECISION, RESOLUTION, AND COVERAGE

We have implemented this retracking algorithm using the ERS-1 Altimeter Waveform Product (WAP, Infoterra Limited, Farnborough, UK, 2001) provided by the European Space Agency at the full 20 Hz sampling rate. These data include the ocean-mode waveforms sampled at 64 range gates. Phases E and F provide an 8-km track spacing at the equator that is needed for construction of 16-km wavelength resolution gravity models. The six repeat cycles from phase G were used to assess the performance of the retracking algorithm.

Waveform data were pre-processed to add the latest orbits and corrections. Precise ERS-1 orbits (Scharroo *et al.* 1998) were used to recompute the latitude, longitude and height of the spacecraft above the WGS84 reference ellipsoid. The CSR4.0 tide model (Bettadpur & Eanes 1994) was computed at each location while the other environmental corrections available on the WAP record were used. For recovery of the gravity field from altimetry, the only corrections that exceed the 1 μrad desired error threshold are due to coastal tides and large orbit error (>2 m). The 550 days of waveform data were

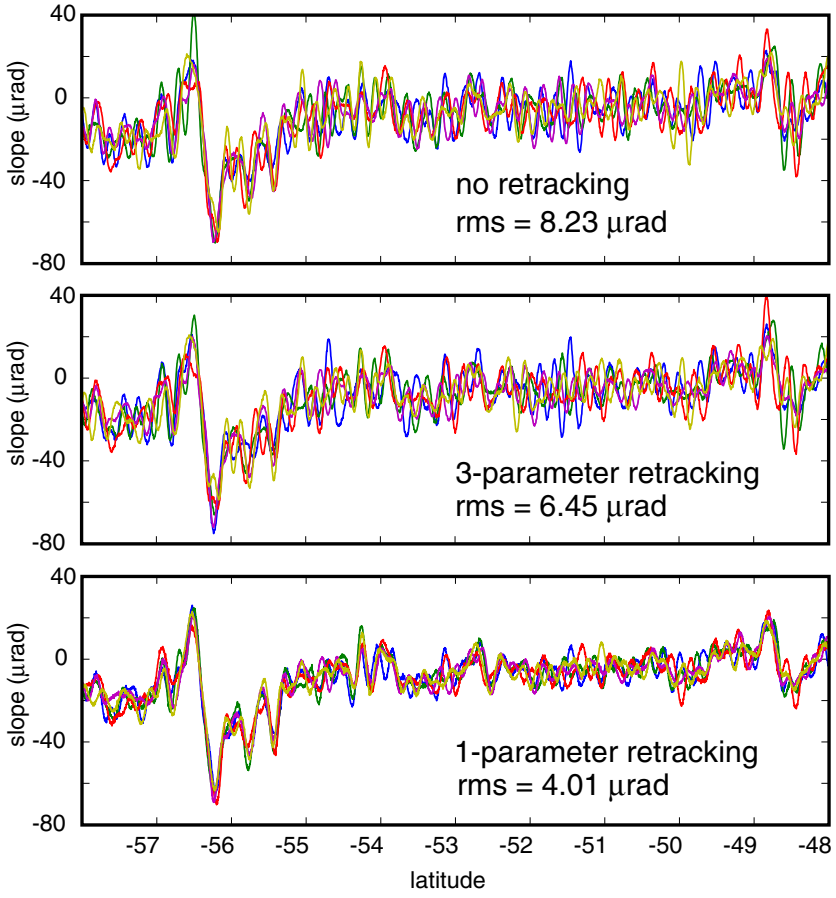

Figure 4. Profiles of along-track sea surface slope for 6 repeat cycles crossing the South Pacific Ocean in a region of generally high SWH. The upper profiles were derived from the onboard tracker available in the waveform data record (rms deviation from model of 8.23 μrad). The middle profiles were derived using a weighted least-squares 3-parameter retracking algorithm as in Monte Carlo experiment 'C' shown in Fig. 2(c) (rms = 6.45 μrad). The lower profiles were derived from a 1-parameter retracking algorithm constrained by smoothing the rise-time and amplitude parameters as in the text (rms = 4.01 μrad).

reformatted into 184-byte records at a 20-Hz sampling rate, which amounts to about 0.5 billion waveforms (95 Gbytes). The three-parameter retracking was performed using a standard non-linear Newton–Raphson iteration where typically five to nine iterations were needed to achieve convergence. The data were segmented into profiles having time gaps no greater than 4 s and low-pass Gaussian filters were applied to the rise-time and amplitude parameters. The data were retracked a second time using the smoothed rise-time and amplitude parameters and solving for the arrival time using a Golden section search in one dimension as implemented in Numerical Recipes (Press *et al.* 1992).

IMPROVEMENTS IN SLOPE ACCURACY AND ALONG-TRACK RESOLUTION

Accuracy and resolution were estimated using the 6 repeat profiles from phase G of the ERS-1 mission. Accuracy was assessed by computing along-track slope for profiles crossing the Pacific ocean over areas of both high and low SWH (Fig. 4). Slope was computed at 20 Hz sampling rate and then low-pass filtered with a 0.5 gain at 18 km to simulate the smoothing filters that are applied when a gravity field is constructed. Slopes based on the arrival-time estimate from the onboard tracker are shown in the top panel and have an rms deviation about the mean profile of 8.23 μrad. Slopes derived from the three-parameter retracking algorithm (centre panel) have an rms deviation of 6.45 μrad while slopes derived from the one-parameter retracking algorithm (lower panel) have an rms deviation of 4.01 μrad. Further analysis shows the greatest improvement in areas of generally high SWH. Although we have not analysed the comparable Ocean Product (OPR V3) for these ERS-1 data, we expect the noise level is similar to the three-parameter retracking results. Thus this new algorithm reduces the rms error to 62 per cent of the rms error for the standard retracking methods which corresponds to a 38 per cent improvement in range precision.

Improvements in along-track slope accuracy translate into improvements in along-track resolution. To assess the resolution improvement we selected two areas for repeat-track analysis that match the two areas used by Yale *et al.* (1995). The first area is the equatorial Atlantic, which has high gravity signal and low oceanographic noise (Fig. 5, top). Coherence between repeat tracks was computed for the three cases of onboard tracking (dotted), three-parameter retrack (dashed line) and one-parameter retrack (solid line). This area shows an improvement in resolution from 36 to 32 km. A similar analysis in the South Pacific, which is an area of low gravity signal and high oceanographic noise, shows an improvement from 43 to 33 km.

Finally, we demonstrate the improvement in altimeter coverage in coastal areas. The test area is the back-arc region between Indonesia and Borneo. This is a challenging area for gravity field recovery from altimetry because the tracks run mainly N–S and the track spacing is greatest at the equator (~8 km). The gravity anomalies have relatively short wavelength and low amplitude in relation to the noise. We plot along-track slope profiles minus EGM96 (Lemoine *et al.* 1998) for two cases—onboard tracking (Fig. 6—left) and retracked (Fig. 6—right). The lower noise level of the retracked data reveals previously unseen gravity signals spanning multiple adjacent tracks; note that both sets of profiles were edited and filtered using the same algorithms. The lower noise level of the retracked data causes fewer data to be edited, especially near the coastline so near-shore coverage is improved.

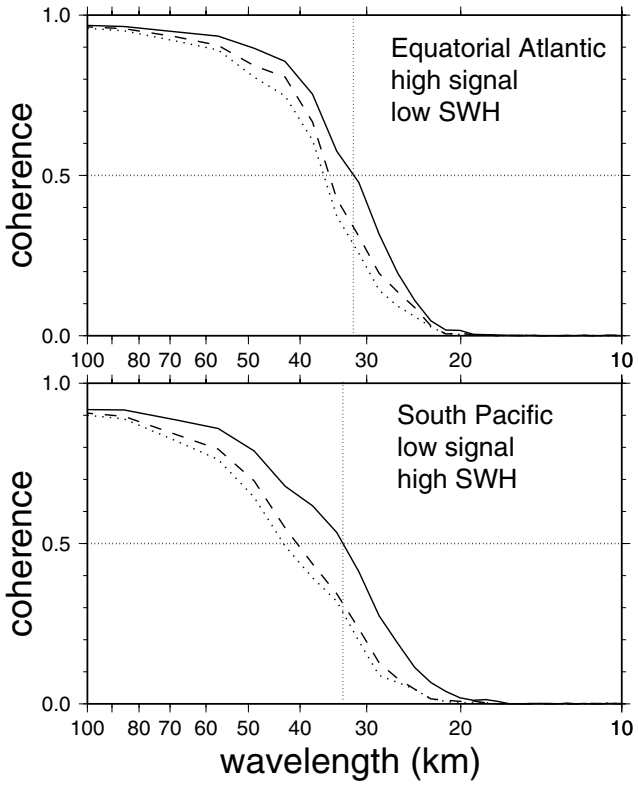

Figure 5. Coherence between repeat altimeter profiles in two areas studied in Yale *et al.* (1995). Dotted curve no retracking, dashed curve 3-parameter retracking, solid curve 1-parameter retracking. Retracking improved the 0.5 coherence from 36 to 32 km in the Equatorial area and from 43 km to 33 km in the South Pacific area. An important result is that the 1-parameter approach yields a wavelength of 0.5 coherence, which is essentially independent of sea state.

Using the retracked ERS-1 data we have also constructed a gravity model and compared the satellite-derived gravity to a ship profile to determine the improvement in accuracy due to retracking (Fig. 7). The comparison with anomalies from gravity model Version 9.1 (no retracking) has a mean difference of 25.3 mGal and an rms difference of 5.62 mGal. Retracking of ERS-1 results in an improved rms of 4.75 mGal. (Non-zero mean differences are expected due to absolute calibration errors in ship gravimetry, Wessel & Watts 1988.) In addition to retracking ERS-1 data we are experimenting with retracking Geosat data and using a least-squares method of biharmonic splines (Sandwell 1987; Wessel & Bercovici 1998) to grid the along-track residual slopes. These combined effects improve the rms misfit to 2.98 mGal. We believe that a more careful treatment of all the non-repeat orbit altimeter data will result in significant improvements in the global marine gravity field.

COMPARISON WITH THE METHOD OF MAUS *ET AL.*

To increase the precision of estimated arrival time, Maus *et al.* (1998) invert 408 waveforms simultaneously to recover 408 estimates of arrival time but constrained to share only a single estimate of rise time. In addition, the 408 arrival-time estimates are coupled, as in a smoothing spline, to guarantee that the power spectrum of the resulting sea surface height will have a desired shape. We believe the key to their approach, which was not highlighted in their study,

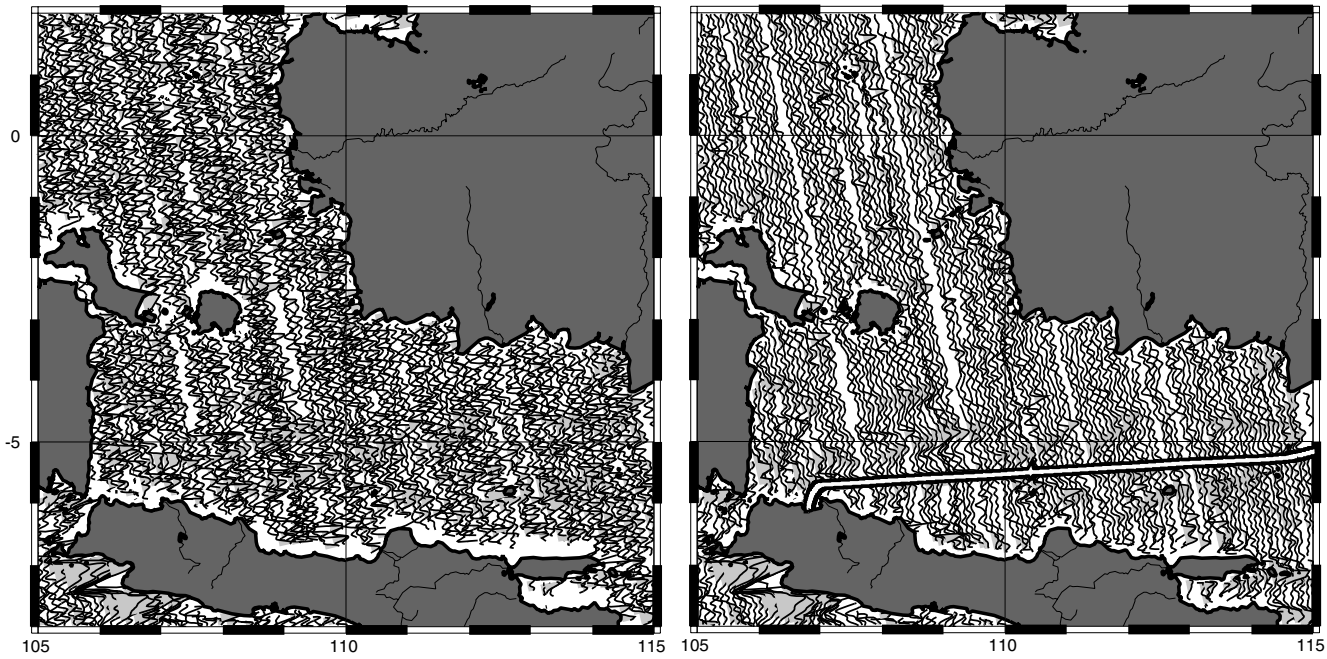

Figure 6. Along-track sea surface slope for ascending profiles from the ERS-1 geodetic phases with the EGM96 model removed. Left—arrival time from onboard tracker, right—arrival time from 1-parameter retracking algorithm. The decrease in noise level reveals gravity lineaments associated with basement structure of this continental margin. Retracking also improves recovery of data near shore. The trackline of the shipboard gravity profile used to assess the accuracy of the satellite-derived gravity is shown in the right panel.

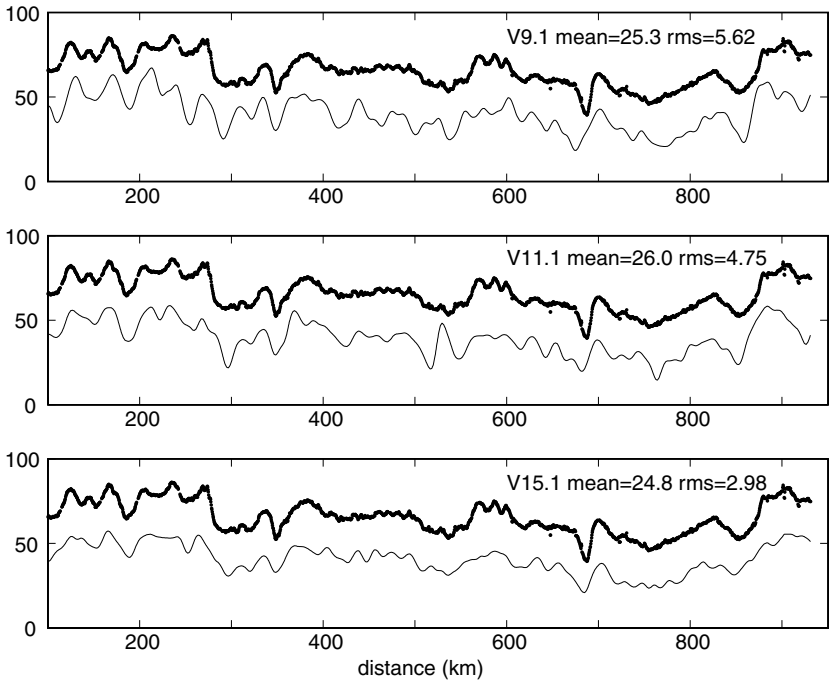

Figure 7. Comparison between satellite-derived gravity models (thin lines) and a shipboard gravity profile (points) across the Java Sea (trackline in Fig. 6). (top) Gravity model version 9.1 does not use retracked altimeter data and has an rms misfit of 5.62 mGal. The mean difference of 25 mGal is due to a mean error commonly found in shipboard gravity (Wessel & Watts 1988). (middle) Gravity model version 11.1 uses retracked ERS-1 altimeter data but the Geosat data were not retracked; the rms misfit is improved by nearly 1 to 4.75 mGal. (bottom) Gravity model version 15.1 is based on both retracked ERS-1 and Geosat altimeter profiles and also used a local least-squares adjustment to simultaneously fit the residual along-track slopes from ERS-1, Geosat, and Topex. The rms is improved further to 2.98 mGal, which is about one-half the rms of the V9.1 gravity field.

is that they force the rise time (i.e. the SWH) to remain constant across a window of 408 points (132 km). Our experiments show that any *a priori* constraint that suppresses freedom for error in rise time will also reduce the error in sea surface height. If the Maus *et al.* (1998) approach were implemented in a running window, it would have the effect of applying a boxcar filter to SWH with a filter width of 132 km. This is similar to our use of a Gaussian filter with a characteristic wavelength of 90 km. We did not find that it was

necessary to simultaneously impose a smoothness constraint on the geoid as performed by Maus *et al.* (1998). Instead we perform the along-track filtering after the retracking process. However, we found that the overall results were improved by simultaneously fitting three waveforms in a moving window to effectively reduce the along-track sampling rate from 20 to 10 Hz.

The Maus *et al.* approach is cumbersome to implement because it requires simultaneous inversion of 408 waveforms with an imposed correlation among the arrival-time parameters to ensure sea surface height smoothness. However, it has the advantage that the retracking only needs to be performed once. Our approach, although it requires a three-step process, is easy to understand and trivial to implement, as the inversion operation works on only one waveform (or a few waveforms) at a time. Furthermore, our scheme allows direct estimation of the resolved correlation scale in the SWH field (Fig. 3) and makes explicitly clear the role of the smoothing applied to the SWH and amplitude parameters.

CONCLUSIONS

The Monte Carlo simulation of altimeter waveforms, as well as the analysis of ERS waveform data, demonstrates an inherent correlation between least-squares estimates of arrival time and rise time. The correlation is caused by the noise properties of the return waveform. Noise is low prior to the arrival of the waveform and increases later in the waveform as more energy scatters off the rough ocean surface. This change in noise introduces the inherent correlation that can mimic true sea-state bias. The correlation is greatest over short length scales ($<$90 km) and can be removed by low-pass filtering SWH along profiles. Most oceanographic studies of repeat altimeter profiles are focused in intermediate and long wavelength variations in height where this correlation is less of a problem. Nevertheless it is likely that some of this correlation is falsely absorbed into the parameterization of the true EM sea state bias.

The noise properties of the return waveform are well understood, so it seems reasonable to perform a weighted least-squares estimate of the waveform parameters. However, simulations show that weighting the fit leads to a more significant correlation between arrival time and rise time with a slope of one (in dimensionless waveform gate width units). This high correlation also increases the error in the arrival time suggesting that a weighted least-squares approach is inferior to the unweighted least-squares approach (Rodriguez 1988). Maus *et al.* (1998) overcome the higher errors introduced by a non-uniform weight function by using a multiple waveform retracking algorithm that solves for a single rise-time parameter and multiple arrival-time parameters. While their approach provides significant improvements in range precision, they left unstated the fundamental assumption of their parameterization: that the rise time (i.e. SWH) varies smoothly along the satellite track. Here we explicitly make this assumption and establish the wavelength of the low-pass filter that is optimal for smoothing the rise time ($\sim$90 km). We argue that the rms-height distribution of waves in the deep ocean will vary smoothly in space due to the high group velocity of the wave trains relative to the speed of the storms that generate the waves. This assumption may become invalid across sharp wind fronts and in shallow coastal areas just seaward of the surf zone.

Our retracking algorithm works on individual waveforms, but three steps are involved. First, a standard three-parameter retracking algorithm is used. Second, the rise-time and amplitude parameters obtained at the first step are low-pass filtered along continuous profiles. Third, the data are retracked again, using the smoothed values from the second step and solving for only the arrival time. Note that fixing the rise time and amplitude to the smoothed values basically fixes the shape of the waveform to agree with surrounding waveforms; this in turn provides stability to the least-squares estimate. Using this approach we obtain a 38 per cent improvement in range precision between the standard three-parameter approach and the one-parameter approach. Moreover, we find that the precision of the arrival time is less sensitive to the SWH. Maus *et al.* (1998) reached a similar conclusion.

Finally we have used this approach to retrack all ERS-1 data for the geodetic phases (E and F) as well as six repeat cycles of phase G. These data were combined with all available Geosat geodetic mission data, Geosat exact repeat mission data and Topex/Poseidon altimetry data to construct a new marine gravity field. The method of combining the along-track slopes is described in Sandwell & Smith (1997). A 1-min grid is available by ftp (version 11.1 at http://topex.ucsd.edu). We have experimented with a similar approach to retrack all of the data from the Geosat Geodetic Mission. Preliminary results are shown in Fig. 7. The value of retracking all of the repeat-track altimetry from Geosat, ERS-1/2 and Topex/Poseidon is unclear. Retracking will certainly improve the short-wavelength precision of the measurements. Moreover, it is possible that this retracking will eliminate the artificial component of the sea state bias and provide a consistent SSB model for all altimeters. However, the long-wavelength accuracy of this retracking approach still needs to be investigated.

ACKNOWLEDGMENTS

The European Space Agency generously provided the raw ERS-1 waveform data through their distributor Infoterra Limited. We thank Helen Fricker for providing software to read the raw ERS waveform data. This research was supported by NASA (NAG5-13673) and the National Science Foundation (NSF OCE-0326707). ConocoPhillips and ExxonMobil provided critical start-up funding the research and continue to support this effort. The contents are solely the opinions of the authors and do not constitute a statement of policy, decision, or position on behalf of NOAA or the US Government.

REFERENCES

Abramowitz, M. & Stegun, I.A., 1972. *Handbook of Mathematical Functions With Formulas, Graphs, and Mathematical Tables*, US Government Printing Office, Washington, DC, p. 1045.

Amarouche, L., Thibaut, P., Zanife, O.Z., Dumont, J.-P., Vincent, P. & Steunou, N., 2004. Improving the Jason-1 ground retracking to better account for attitude effects, *Marine Geodesy,* **27,** 171–197.

Bettadpur, S.V. & Eanes, R.J., 1994. Geographical representation of radial orbit perturbations due to ocean tides: Implications for satelliye altimetry, *J. geophys. Res.,* **99**(C12), 24 883–24 898.

Brown, G.S., 1977. The average impulse response of a rough surface and its application, *IEEE Transactions on Antenna and Propagation,* AP-**25**(1), 67–74.

Chelton, D.B., Reis, J.C., Haines, B.J., Fu, L.L. & Callahan, P.S., 2001. Satellite altimetry, in *Satellite Altimetry and Earth Sciences,* pp. 1–131, eds. Fu, L.L. & Cazenave, A., Academic Press, San Diego.

Dumont, J.-P., 1985. Estimation Optimale des Parametres des Signaux Radar Poseidon, Institut National Polytechnique de Toulouse, Toulouse, France.

Hayne, G.S., 1980. Radar altimeter mean return waveforms from near-normal-incidence ocean surface scattering, *IEEE Transactions on Antennas and Propagation,* AP-**28**(5), 687–692.

Hayne, G.S., Hancock, D.W., Purdy, C.L. & Callahan, P.S., 1994. The corrections for significant wave height and altitude effects in the TOPEX radar altimeter, *J. geophys. Res.,* **99**(NC12), 24 941–24 955.

Lemoine, F.G. *et al.*, 1998. The development of the joint NASA CSFC and the national Imagery and Mapping Agency (NIMA) geopotential model EGM96. NASA/TP-1998-206861, Goddars Space Flight Center, NASA, Greenbelt, Maryland.

MacArthur, J.L., Marth, J.P.C. & Wall, J.G., 1987. The Geosat radar altimeter, *Johns Hopkins APL Technical Digest,* **8**(2), 176–181.

Maus, S., Green, C.M. & Fairhead, J.D., 1998. Improved ocean-geoid resolution from retracked ERS-1 satellite altimeter waveforms, *Geophys. J. Int.,* **134**(N1), 243–253.

Monaldo, F., 1988. Expected differences between buoy and radar altimeter estimates of wind speed and significant wave height and their implications on buoy-altimeter comparisons, *J. geophys. Res.,* **93**(C3), 2285–2302.

Press, W.H., Teukolsky, S.A., Vetterling, W.T. & Flannery, B.P., 1992. *Numerical recipes in C,* 2nd edn, Cambridge University Press, New York, p. 994.

Raney, R.K., Smith, W.H.F. & Sandwell, D.T., 2004. Abyss-Lite: *A High-Resolution Gravimetric and Bathymetric Mission*. American Institute of Aeronautics and Astronautics, San Diego, pp. 1–5.

Rodriguez, E., 1988. Altimetry for non-Gaussian oceans: Height biases and estimation of parameters, *J. geophys. Res.,* **93,** 14 107–14 120.

Rodriguez, E. & Martin, J.M., 1994. Assessment of the TOPEX altimeter performance using waveform retracking, *J. geophys. Res.,* **99**(C12), 24 957–24 969.

Sandwell, D.T., 1987. Biharmonic spline interpolation of Geos-3 and Seasat altimeter data, *Geophys. Res. Lett.,* **14**(2), 139–142.

Sandwell, D.T. & Smith, W.H.F., 1997. Marine gravity anomaly from Geosat and ERS-1 satellite altimetry, *J. geophys. Res.,* **102**(B5), 10 039–10 054.

Scharroo, R. & Lillibridge, J., 2005. Non-Parametric sea-state bias models and their relevance to sea level change studies, *Proc. of the 2004 Envisat & ERS Symposium,* Salzburg, Austria.

Scharroo, R., Visser, P.N.A.M. & Mets, G.J., 1998. Precise orbit determination and gravity field improvement for the ERS satellites, *J. geophys. Res.,* **103**(C4), 8113–8127.

Smith, W.H.F. & Sandwell, D.T., 1997. Global sea floor topography from satellite altimetry and ship depth soundings, *Science,* **277**(26 September), 1956–1961.

Stewart, R.H., 1985. *Methods of Satellite Oceanography,* Univ. of Calif. Press, Berkley, California, p. 360.

Wang, Y.M., 2000. The satellite altimeter data mean sea surface GSFC98, *Geophys. Res. Lett.,* **25**(5), 701–704.

Wessel, P. & Bercovici, D., 1998. Interpolation with splines in tension: a Green's function approach, *Mathematical Geology,* **30**(1), 77–93.

Wessel, P. & Watts, A.B., 1988. On the accuracy of marine gravity measurements, *J. geophys. Res.,* **93**(B1), 393–413.

Yale, M.M., Sandwell, D.T. & Smith, W.H.F., 1995. Comparison of along-track resolution of stacked Geosat, ERS-1 and TOPEX satellite altimeters, *J. geophys. Res.,* **100**(B8), 15 117–15 127.

APPENDIX A: THE EFFECT OF ERS-1 HARDWARE TRUNCATION ON THE EXPECTED MEAN AND VARIANCE OF WAVEFORM GATE SAMPLES

The ERS-1 spacecraft transmitted radar pulses with a pulse repetition frequency of 1020 Hz. Fifty consecutive waveforms were accumulated on-board in hardware to form a quasi-average waveform, and only these quasi-average waveforms were telemetred to the ground for processing. Unfortunately the reported quasi-average waveform is not precisely the arithmetic mean of the received and gated values,

$$\bar{P} = \frac{1}{50}\sum_{k=1}^{50} P_k.$$

Instead, to prevent the sum from overflowing the hardware, the following formula was used to accumulate the average waveform power:

$$\tilde{P} = \sum_{k=1}^{50} \text{floor}(P_k/50).$$

where 'floor(x)' in the above expression is the greatest integer less than or equal to x. This appendix explores the probability distributions for P, $\bar{P}$ and $\tilde{P}$.

The probability distribution for the power in a returned radar pulse, P

The radar signal received by an altimeter has contributions from many randomly distributed radar scatterers on the ocean surface. The phase from each scatterer is uniformly and randomly distributed (Brown 1977). The in-phase (C) and quadrature (S) components of the received signal are each the sum of a large number of random variables; therefore C and S have Gaussian distributions with zero mean and equal variance. The relative phase of C and S, that is, $\phi =$ atan2 (S, C), is uniformly and randomly distributed. The altimeter detects the power of the returned waveform: $P = C^2 + S^2$. P is thus a random variable that, apart from a scale factor, is distributed as chi-square with two degrees of freedom, χ_2^2, that is, it has an exponential distribution, in which the standard deviation is equal to the mean. If the expected value of P is $\hat{P}$ then the variance of P is $\hat{P}^2$.

Factors affecting the distribution of a sequence of 50 returned pulses

Traditional radar altimeters such as ERS-1 do not have a high enough sampling rate to operate in a synthetic aperture mode (i.e. along track spacing $<1/2$ antenna diameter) so each returned waveform may be considered independent realization of the ocean surface. Over $1/20$ of a second, the ocean wave height distribution, density of scatterers on the surface, delay and attenuation of energy along the propagation path and antenna pointing should not change appreciably. Therefore during the acquisition of 50 consecutive pulses the expected returned power, $\hat{P}$, should depend only on the receive time relative to the return onset time: $\hat{P} = \hat{P}(t - t_0)$. Hereafter, we will assume that the radar instrument is tracking correctly, so that each of the waveforms in a sequence of 50 is correctly aligned, meaning that the waveform sample gates are distributed around t_0 with the same distribution as each pulse is sampled by the waveform gates. These conditions will ensure that the expected value of the power in any one waveform gate is a constant during the acquisition of 50 consecutive waveforms. Each of the 50 waveforms then is independently and identically distributed, by virtue of the short decorrelation time and the proper tracking.

The distribution of the arithmetic mean of 50 returned values, $\bar{P}$

The arithmetic mean $\bar{P}$ is a linear combination of 50 random variables and so should have an approximately Gaussian distribution,

by the central limit theorem. More precisely, the distribution of $\bar{P}$ is, apart from a scale factor again, that of chi-square with 100 degrees of freedom; however, the distribution of χ^2_{100} is very well approximated by a Gaussian distribution (Abramowitz & Stegun 1972, section 26.4.11 and following). $\bar{P}$ is an unbiased estimator; its expected value is $\hat{P}$. This can be found directly by taking the expectation of the equation for $\bar{P}$, or by appropriately scaling the χ^2_{100} distribution, or simply making use of the fact that the arithmetic mean is unbiased. The variance of $\bar{P}$ obtained by scaling the χ^2_{100} distribution is the same as would be found by the Gaussian approximation: $\mathrm{Var}\{\bar{P}\} \approx \mathrm{Var}\{P\}/50 = \hat{P}^2/50$. This means that the expected standard deviation in a mean waveform $\bar{P}$ is roughly $1/7$ of $\hat{P}$.

The properties of the quasi-average, $\tilde{P}$

Applying again the assumptions that each P_k is independent and identically distributed one reasons that the distribution for $\tilde{P}$ must have a Gaussian form for any $\hat{P}$. This justifies the use of least-squares fitting techniques in retracking. However, the 'floor' operation effectively applies an unpredictable scale factor to each P_k in the quasi-average $\tilde{P}$, and it is not immediately obvious how this will affect the expectation (mean) $\mu = E\{\tilde{P}\}$ and variance $\sigma^2 = \mathrm{Var}\{\tilde{P}\}$.

We estimated the mean and variance of $\tilde{P}$ as functions of the expected true power, $\hat{P}$, by Monte Carlo experiments as follows. We generated pseudo-random deviates X_k uniformly distributed in the interval (0, 1). From these we obtained exponentially distributed, unit mean deviates Y_k by the logarithmic transformation $Y_k = -\log(X_k)$ (Press *et al.* 1992, Section 7.2). By simply scaling $P_k = \hat{P}Y_k$ we generated quasi-random numbers P_k having the correct distribution for realizations of a single waveform pulse gate sample with expected power level $\hat{P}$. It is then straightforward to form many realizations of $\tilde{P}$ and compute the sample mean and standard deviation of these realizations. Graphs of the bias $E\{\tilde{P}\} - \hat{P}$ and the standard deviation $\sigma(\hat{P})$ are shown as Fig. A1. The bias is zero when $\hat{P}$ is zero, of course, but quickly approaches a steady value of -23. Note that this is slightly less than half of the truncation factor of 50, probably reflecting the asymmetry in the exponential distribution of the P_k; the expected difference between rounding and truncating a symmetric distribution would be half the truncation factor. The standard deviation is slightly less than the theoretical value of $\hat{P}/\sqrt{50}$, perhaps also due to the exponential distribution.

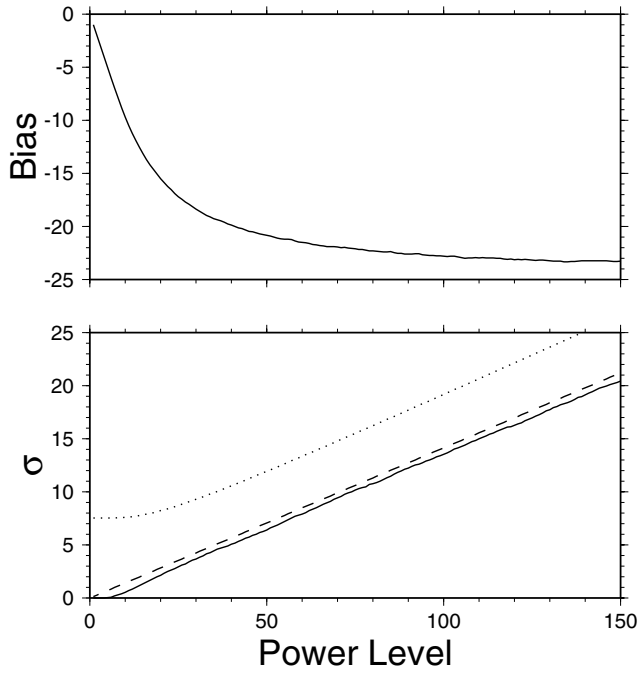

Figure A1. Top: The bias (expected value of the quasi-mean power level, $\tilde{P}$, minus the correct true mean power level, $\hat{P}$) as a function of the true mean power level, $\hat{P}$. The asymptotic value of the bias is -23. Bottom: The standard deviation of the quasi-mean power level (solid line) is slightly less than the standard deviation of the true theoretical population (dashed line, equal to $\hat{P}/\sqrt{50}$). The dotted line shows the least-squares weight used in this paper, $(\tilde{P} + 50)/\sqrt{44}$ as a function of $\hat{P}$. Experimentation showed that this weight gave the best results. It is somewhat higher than the actual standard deviation to avoid overweighting the lowest power levels and to account for a background thermal noise level that is missing from the waveforms because of their truncation at low amplitude.